Neoplasia • Vol. 8, No. 5, May 2006, pp. 402–412 402

www.neoplasia.com

Cardenolide-Induced Lysosomal Membrane Permeabilization Demonstrates Therapeutic Benefits in Experimental Human Non–Small Cell Lung Cancers[1]

Tatjana Mijatovic, Véronique Mathieu*, Jean-François Gaussin†, Nancy De Nève†, Fabrice Ribaucour†, Eric Van Quaquebeke†, Patrick Dumont†, Francis Darro† and Robert Kiss**

*Laboratory of Toxicology, Institute of Pharmacy, Free University of Brussels, Brussels, Belgium; †Unibioscreen SA, Brussels, Belgium

Abstract

Non–small cell lung cancers (NSCLCs) are the leading cause of cancer deaths in most developed countries. Targeting heat shock protein 70 (Hsp70) expression and function, together with the induction of lysosomal membrane permeabilization (LMP), could overcome the multiple anti–cell death mechanisms evidenced in NSCLCs that are responsible for the failure of currently used chemotherapeutic drugs. Because cardenolides bind to the sodium pump, they affect multiple signaling pathways and thus have a number of marked effects on tumor cell behavior. The aim of the present study was to characterize *in vitro* and *in vivo* the antitumor effects of a new cardenolide (UNBS1450) on experimental human NSCLCs. UNBS1450 is a potent source of *in vivo* antitumor activity in the case of paclitaxel- and oxaliplatin-resistant subcutaneous human NCI-H727 and orthotopic A549 xenografts in nude mice. *In vitro* UNBS1450-mediated antitumor activity results from the induction of nonapoptotic cell death. UNBS1450 mediates the decrease of Hsp70 at both mRNA and protein levels, and this is at least partly due to UNBS1450-induced downregulation of NFAT5/TonEBP (a factor responsible for the transcriptional control of Hsp70). These effects were paralleled by the induction of LMP, as evidenced by acridine orange staining and immunofluorescence analysis for cathepsin B accumulation.

Neoplasia (2006) **8,** 402–412

Keywords: NSCLCs, cardenolides, antitumor agent, Hsp70, lysosomal membrane permeabilization.

Introduction

Non–small cell lung cancers (NSCLCs) are the leading cause of cancer deaths in most developed countries and have an overall 5-year survival rate of as low as 15% because adjuvant chemotherapy (including camptothecin, taxane, platin, and vinca alkaloid derivatives) has only a limited therapeutic effect [1,2]. The successful treatment of cancer with chemotherapy is largely dependent on the ability of the treatment to trigger cell death in tumor cells. Most tumor cells (including NSCLC cells) are naturally resistant to not only apoptotic-related cell death [type I programmed cell death (PCD)] but also non–apoptotic-related types such as necrosis, autophagy (type II PCD), senescence, mitotic catastrophe, and paraptosis [3–6]. NSCLCs are naturally chemoresistant because they express a large set of proteins (such as cyclooxygenase-2, prostaglandin E synthetase, ornithine decarboxylase, lung-related resistance protein, and glutathione *S*-transferases α, μ, and π) that counteract chemotherapeutic insults [7]. Resistance to cell death in NSCLCs also relates to constitutive activation of the phosphatidylinositide 3-kinase [8], Akt [9,10], and NF-κB [10] signaling pathways, all of which are interlinked [10,11].

In a previous study [12], we were able to demonstrate that a cardenolide-related compound (UNBS1450) could constitute a potential weapon against human experimental NSCLCs. Cardenolides (e.g., ouabain and digitoxin) bind to the sodium pump (i.e., Na^+/K^+ ATPase), which is an energy-transducing ion pump that uses energy derived from the hydrolysis of ATP to maintain a high K^+ concentration and a low Na^+ concentration in the cytoplasm, which, in turn, provides the driving force for the net movement of other substances such as glucose, amino acids, Ca^{2+}, and H^+ [13–16]. Through their binding to the sodium pump, cardenolides have a marked effect on tumor cell behavior and affect several downstream signaling pathways, including those of Src kinases, epidermal growth factor receptor (EGFR), Ras, p42/p44 mitogen-activated protein kinases, and NF-κB [15,16]. UNBS1450 is able to deactivate highly activated NF-κB pathways in A549 NSCLC cells by acting simultaneously at several points along this pathway [12]. Indeed, the UNBS1450-induced deactivation of the NF-κB pathways includes both the inhibitory I-κB portion of the NF-κB signaling pathway and its stimulatory p65/Rel-A NF-κB portion [12]. UNBS1450-induced effects at the inhibitory I-κB protein level involve: 1) the upregulation of inhibitory protein expression (as observed for I-κBβ); 2) the downregulation of

Abbreviations: Hsp70, heat shock protein 70; LMP, lysosomal membrane permeabilization

Address all correspondence to: Robert Kiss, PhD, Laboratory of Toxicology, Institute of Pharmacy, Université Libre de Bruxelles Campus Plaine, CP 205/1, Boulevard du Triomphe, Brussels 1050, Belgium. E-mail: rkiss@ulb.ac.be

[1]This work was supported by grants awarded by the *Fonds Yvonne Boël* (Brussels, Belgium) and the *Région de Bruxelles-Capitale* (Brussels, Belgium). R.K. is Director of Research at *Fonds National de la Recherche Scientifique* (Belgium).

DOI 10.1593/neo.05850

the phosphorylation levels of I-κBα; and 3) the downregulation of the expression of cdc34 [12]. UNBS1450-induced effects at the p65/Rel-A NF-κB level include: 1) the downregulation of the expression levels of p65; 2) the downregulation of the DNA-binding capacity of the p65 subunit; and 3) the downregulation of NF-κB transcriptional activity [12].

Polypeptides belonging to the heat shock protein 70 (Hsp70) major stress protein family interact with the NF-κB multifunctional regulatory complex in cellular defense mechanisms [17]. In fact, with its ability to bind with a high level of affinity to the plasma membrane, Hsp70 elicits rapid intracellular calcium flux and activates NF-κB [18]. It has recently been shown that Hsp70 and NF-kB are intimately linked in the roles that they play in cancer cell migration [19,20]. One of the anti–cell death mechanisms that is active in lung cancer cells involves the overexpression of Hsp70 as it fulfills its prosurvival function by inhibiting lysosomal membrane permeabilization (LMP) [21,22]. Frese et al. [21] have shown that the selective downregulation of Hsp70 induces massive caspase-independent tumor cell death in lung cancer, but not in normal lung cells. Accumulating data now show that lysosomes also function as death signal integrators that mediate caspase-independent and/or apoptosis-inducing factor–independent PCD (for a review, see Jaattela [23] and Fehrenbacher and Jaattela [24]).

The aim of the present study was to pursue our previous investigations [12] into the *in vitro* and *in vivo* antitumor effects of UNBS1450, a hemisynthetic derivative of 2″-oxovoruscharin (UNBS1244; Figure 1) [25], in the case of human NSCLC models. In this study, we focus on UNBS1450-mediated effects on Hsp70 expression and LMP-related cell death.

Materials and Methods

Compounds

The drugs used were as follows: ouabain (Acros Organics, Geel, Belgium), digitoxin (Acros Organics), paclitaxel (Taxol; S. A. Bristol-Myers Squibb, Brussels, Belgium), irinotecan (Campto; Aventis, Brussels, Belgium), SN-38 (7-ethyl-10-hydroxycamptothecin; Aventis), oxaliplatin (Oxaliplatin; Inter-Chemical Ltd., ShenZhen, China), cisplatin (Platinol; S. A. Bristol-Myers Squibb), and carboplatin (Paraplatin; S. A. Bristol-Myers Squibb). As detailed elsewhere [25], UNBS1244 was chemically extracted from the bark of *Calotropis procera*, an African plant. *C. procera* specimens were provided by Prof. Pierre Guissou (Laboratory of Toxicology, University of Ouagadougou, Ouagadougou, Burkina Faso). UNBS1450 was obtained from UNBS1244 by hemisynthesis at the laboratory facility of Unibioscreen SA (Brussels, Belgium) (Figure 1) [25].

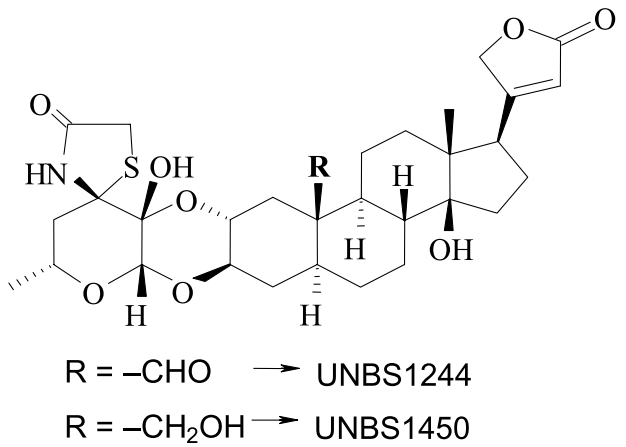

Figure 1. *Chemical structures of UNBS1244 and its hemisynthetic derivative, UNBS1450. The manner in which UNBS1244 was identified in the African plant C. procera and the hemisynthesis of UNBS1450 from UNBS1244 are described in detail in Van Quaquebeke et al. [25].*

Cell Lines

The A549 (code CCL-185) and A427 (code HTB-53) cell lines were obtained from the American Type Culture Collection (Manassas, VA) and were maintained in minimum essential medium (MEM) supplemented with 5% fetal bovine serum. CAL-12T cells, which were obtained from the DSMZ Animal Cell Line Database (code ACC-443; DSMZ, Brunswick, Germany), were maintained in OptiMEM medium supplemented with 5% fetal bovine serum. NCI-H727 cells were obtained from the European Collection of Cell Cultures (code ECACC 94060303; Sigma-Aldrich, Bornem, Belgium) and were maintained in RPMI medium supplemented with 10% fetal bovine serum. All media were supplemented with a mixture of 0.6 mg/ml glutamine (GibcoBRL/Invitrogen SA, Merelbeke, Belgium), 200 IU/ml penicillin (GibcoBRL), 200 IU/ml streptomycin (GibcoBRL), and 0.1 mg/ml gentamycin (GibcoBRL). Trypsin–EDTA, fetal bovine serum, cell culture media, and their supplements were obtained from GibcoBRL/Invitrogen SA. Fetal bovine serum was heat-inactivated for 1 hour at 56°C. All cells were incubated in a 5% CO_2 atmosphere at 37°C in sealed (air-tight) Falcon plastic dishes (Nunc/Invitrogen SA, Merelbeke, Belgium).

In Vitro Overall Growth Determination

Overall cell growth was assessed by 3-[4,5-dimethylthiazol-2yl]-diphenyltetrazolium bromide (MTT) (Sigma, Bornem, Belgium) colorimetric assay, as detailed elsewhere [26]. The tumor cells were incubated for 72 hours in the presence (or in the absence; control) of various drugs at concentrations ranging between 10^{-9} and 10^{-5} M (with semi-log concentration increase). The experiments were carried out in sextuplicate.

Flow Cytometry Analyses for Determining Apoptotic-Related Versus Non–Apoptotic-Related Cell Death and Cell Cycle Kinetics

Flow cytometry analyses of apoptotic-related *versus* non–apoptotic-related cell death were performed according to the experimental protocol detailed by Darzynkiewicz et al. [27]. Briefly, after various treatments with UNBS1450 (Figure 4, *A* and *B*), the cells were incubated in darkness in Annexin V–FITC (V)–propidium iodide (PI) solution for 15 minutes at 4°C (Annexin V–FITC kit; Immunotech, Marseilles, France). Data from around 10,000 cells were

recorded on a logarithmic scale for each sample. XL System II (Beckman Coulter, Miami, FL) was used to give a precise definition of both the percentage of cells in the apoptotic and/or nonapoptotic compartments and the percentage of normal cells (i.e., those apparently left unaffected by UNBS1450 treatment). The so-called normal cells were negative for both Annexin V and PI staining, whereas the apoptotic cells were positive for Annexin V but were negative for PI. The nonapoptotic cells (whose cell membranes have holes) were positive for both PI and Annexin V [23]. Each experiment was carried out in triplicate. Additional experiments aiming to rule out UNBS1450-induced apoptotic effects on human A549 NSCLC cells were carried out by the terminal deoxynucleotidyl transferase deoxyuridine triphosphate nick-end labeling (TUNEL) technique, using an experimental protocol detailed elsewhere [28]. Briefly, A549 cells were treated for 72 hours with UNBS1450 at a concentration of 10 nM or were incubated with the solvent alone. As positive control for apoptosis, A549 cells were incubated for 72 hours with 2.5 μM doxorubicin. Apoptosis was assessed by a flow cytometry–based TUNEL assay. At indicated time points, both nonadherent and adherent cells were harvested and pooled, and fixed overnight (15 hours) with 1% paraformaldehyde (1 hours) and 70% ethanol. On the next day, the cells were processed using APO-BRDU kit (Sigma-Aldrich), according to the manufacturer's instructions. Analysis was performed immediately after the staining reaction on an Epics XL MCL flow cytometer (Beckman Coulter) equipped with a 488-nm argon laser. Apoptosis was quantified by following the increase in FITC dUTP labeling, as against control cells (solvent alone).

The cell cycle kinetics of A549 cells, either treated with UNBS1450 or left untreated (Figure 4*F*), was determined by flow cytometry analyses of PI nuclear staining, using a previously detailed methodology [29].

Flow Cytometry Analyses for Acridine Orange Staining

Acridine orange staining was carried out as an indicator of lysosomal leakage, as described by Nylandsted et al. [22].

Immunofluorescence Analyses for Cathepsin B Expression

As an indicator of lysosomal leakage, cathepsin B immunostaining was carried out using the monoclonal anti–cathepsin B antibody (1:50) provided by Oncogene Research/VWR International (Leuven, Belgium). Human A549 NSCLC cells were fixed and permeabilized as described by Nylandsted et al. [22]. Immunoflourescence analyses were performed in this study as detailed by Mathieu [30].

Total RNA Extraction

Total RNA from the A549 cell line was prepared using the TRIzol isolation reagent (GibcoBRL/Life Technologies/Invitrogen SA, Merelbeke, Belgium), according to the manufacturer's instructions. The RNA extracted was treated with DNase I (GibcoBRL/Life Technologies/Invitrogen SA) to eliminate any remaining genomic DNA. The quantity of RNA was measured by spectrophotometric analysis at 260 nm (Beckman Coulter DU 640; Analis, Ghent, Belgium). The quality and the integrity of the extracted RNA were assessed both by BioAnalyser 2100 (Agilent, Toulouse, France) and by gel electrophoresis in 1% agarose TAE gels (Invitrogen SA), and were visualized by ethidium bromide staining under UV light.

Northern Blot Analyses for Hsp70

Ten micrograms of RNA samples was denatured in 100% formamide. Glyoxal (0.7 M, final concentration) and bromophenol blue were added to the samples, which were then heated at 65°C for 10 minutes, after which they were subjected to electrophoresis in a 1.2% agarose dissolved in Tris/acetate, an EDTA buffer. Electrophoresis was performed at 80 V (4 V/cm) for 120 minutes. Transfer to a nylon membrane (Hybond-N^+; Amersham Pharmacia Biotech Benelux, Roosendaal, The Netherlands) was accomplished electrophoretically, and the RNA was cross-linked by UV irradiation. Blots were hybridized with a DNA probe generated by polymerase chain reaction. The Hsp70 fragment was produced by a standard reverse transcription–polymerase chain reaction using the primers provided by Life Technologies/Invitrogen SA. These primers were selected using HYBSIMULATOR software (Advanced Gene Computing Technology, Irvine, CA). The primers were 5′-TTGAGGGCATCGACTTC-3′ (forward) and 5′-CTCGTACACCTGGATCAG-3′ (reverse). The 470-bp fragment so generated was purified using the High Pure PCR Product Purification Kit (Roche Diagnostics, Mannheim, Germany), in accordance with the manufacturer's instructions. The probe was generated by a radiolabeling process using random primer technique, in conjunction with a commercially available kit (Rediprime II; Amersham Pharmacia Biotech Benelux), in the presence of [α-^{32}P] dCTP (Amersham Pharmacia Biotech Benelux). The probe was purified using a QuickSpin DNA Sephadex column (Roche Diagnostics), and the rate of incorporation was quantified by scintillation counting. The membrane was subsequently hybridized overnight at 65°C (Rapid-hyb Solution; Amersham Pharmacia Biotech Benelux). After stringent washing, the hybridization results were visualized using a Fuji-BAS5000 scanner and an AIDA image analyzer software (Raytest Benelux, Tilburg, The Netherlands).

Western Blot Analyses

Cell extracts were prepared by directly lysing subconfluent A549 cells in a boiling lysis buffer (10 mM Tris, pH 7.4; 1 mM Na_3O_4V; 1% sodium dodecyl sulfate, pH 7.4). Forty micrograms of proteins (evaluated by bicinchoninic acid (BCA) protein assay; Pierce/PerbioScience, Erembodegem, Belgium) was loaded onto a denaturing polyacrylamide gel. Following electrophoresis, the proteins were blotted onto a Polyscreen*PVDF membrane (NEN; Life Science Products, Boston, MA). The proteins of interest were immunodetected by specific affinity-purified primary antibodies (in Tris-buffered saline (TBS) containing 0.1% Tween-20 and 5% fat-free dry milk powder or bovine serum albumin), in conjunction with a secondary antibody in the shape of immunoglobulin (Ig) G conjugated with horseradish peroxidase. Control experiments included the omission of the incubation step with the primary antibodies (negative control). Equal loading was verified by

the bright red coloration of the membranes. The integrity and the quantity of the extracts were assessed by tubulin immunoblotting. The primary antibodies were: 1) Hsp70 (1:500) (CST Technologies, Westburg, Leusden, The Netherlands); 2) tubulin (1:3000) (AbCam, Cambridge, UK); and 3) poly(ADP-ribose) polymerase (PARP; 1:250) (BD PharMingen, Erembodegem, Belgium). The secondary antibodies used were as follows: antimouse and antirabbit IgG (Pierce/PerbioScience) and antirat (AbCam). The blots were developed using the Pierce Supersignal Chemiluminescence system (PerbioScience).

Measurements of UNBS1450-Induced Effects on Sodium Pump Activity

Porcine cerebral cortex sodium potassium ATPase activity was measured using an enzyme-linked assay in which the formation of ADP by ATPase was coupled to NADH oxidation in the presence of the enzymes pyruvate kinase and lactate dehydrogenase, with the intermediate substrate phosphoenolpyruvate present in excess [25]. The samples (3×10^{-3} U of porcine Na^+/K^+ ATPase; Sigma-Aldrich) were preincubated for 30 minutes at 37°C in 30 mM Tris–HCl (pH 7.4) and 5 mM $MgCl_2$, with increasing inhibitor concentrations. The reaction was then initiated by the addition of 1 ml of a reaction mixture, which contained (in mM or appropriate units): Tris–HCl (pH 7.4), 30; NaCl, 100; KCl, 5; $MgCl_2$, 5; ATP (Sigma-Aldrich), 3; PEP (Calbiochem/VWR International, Leuven, Belgium), 1; NADH (Calbiochem), 0.3; EGTA (Sigma-Aldrich), 0.1; lactate dehydrogenase (Sigma-Aldrich), 5; and pyruvate kinase (Sigma-Aldrich), 6, with corresponding inhibitor concentrations. Absorbance was measured at 340 nm after 1-hour incubation at 37°C in a 1-ml cuvette (VWR International). The procedure was characterized using an inhibitor range from 1 to 50,000 nM UNBS1450, ouabain, and digitoxin.

In Vivo Subcutaneous Grafting of NCI-H727 and Orthotopic Grafting of Human A549 NSCLC Cells

Potential *in vivo* UNBS1450-related therapeutic effects were determined in nude mice with human NCI-H727 subcutaneous xenografts or A549 orthotopic xenografts by chronic (12 times) intraperitoneal administration of UNBS1450 thrice a week, for four consecutive weeks. The maximum tolerated dose (MTD) for UNBS1450 (and for the other compounds under study) was determined by administering it acutely (in one single intraperitoneal dose) to healthy animals (not grafted with tumors). The survival periods and the weights of the animals were recorded for up to 28 days after the injection of the compound. Eight different doses of UNBS1450 (i.e., 2.5, 5, 10, 20, 40, 80, 120, and 160 mg/kg) were used for the determination of the MTD index. The MTD index is defined as the concentration that kills at least one mouse in a group of three after a minimum of 28 days. The acute MTD for UNBS1450 through the intraperitoneal route was 120 mg/kg (for the MTDs of all compounds used in this study, refer to Figure 2*A*).

Subcutaneous NCI-H727 xenografts were realized by grafting 2×10^6 human NCI-H727 cells onto the left flank of 8-week-old female nu/nu mice (weight, 21–23 g; Bio-Services, Uden, The Netherlands). Tumor size was measured as previously described [31] (i.e., twice weekly, using a caliper) and is expressed in areas (mm^2) by multiplying the two largest perpendicular diameters. Based on this, we were able to evaluate potential UNBS1450-induced decreases in tumor growth rates (i.e., drug-induced tumor surface inhibition).

Orthotopic A549 xenografts were obtained by grafting 2×10^6 human A549 cells through the thorax into the left-hand side of the lungs of the nude mice (see NCI-H727 xenografts), as detailed elsewhere [7]. All orthotopic grafts were performed under anesthesia [saline, Rompun (Bayer, Leverkusen, Germany), and Imalgene (Merial, Lyons, France), 5:1:1, vol/vol/vol]. Highly reproducible tumor developments (100%) were obtained for both NCI-H727 and A549 tumor grafts in each experiment.

For ethical reasons, the endpoint of the NCI-H727–related experiments was the sacrifice (in a CO_2 atmosphere) of all subcutaneous xenograft-bearing nude mice on the 49th day after tumor graft because the mean tumor size had reached 500 mm^2 in the control group. The endpoint of the A549-related experiments was the recording of the survival period of each of the A549 NSCLC–bearing nude mice. For ethical reasons, each animal was submitted to euthanasia (in a CO_2 atmosphere) when it had lost 20% of its weight taken at the time of the tumor graft. As detailed elsewhere, autopsy and histology were performed on each mouse to confirm the presence of tumor development [7]. All *in vivo* experiments described in the current study were performed based on authorization no. LA1230509 of the Animal Ethics Committee of the Belgian Federal Department of Health, Nutritional Safety, and the Environment.

Statistical Analyses

Statistical comparisons between the control group and the treated group were performed by first carrying out the Kruskal-Wallis test (a nonparametric one-way analysis of variance) and, where this test revealed significant differences, we investigated whether any of the groups treated differed from controls. For this purpose, we applied the Dunn's multiple comparison procedure (two-sided test), which was adapted to the comparison of treatments and controls [i.e., where only $(k - 1)$ comparisons were carried out among the k groups tested by the Kruskal-Wallis test, instead of the possible $k(k - 1)/2$ comparisons considered in the general procedure]. Survival analysis was carried out using Kaplan–Meier curves and the Gehan generalized Wilcoxon test. All statistical analyses were carried out using Statistica software (Statsoft, Tulsa, OK).

Results

UNBS1450 Is a Cardenolide with Marked In Vitro Antitumor Activities in the Case of Human NSCLC Cell Lines

UNBS1244 is a novel cardenolide that we identified in African specimens of *C. procera* [25]. UNBS1450, which is a hemisynthetic derivative of UNBS1244 [25], differs from

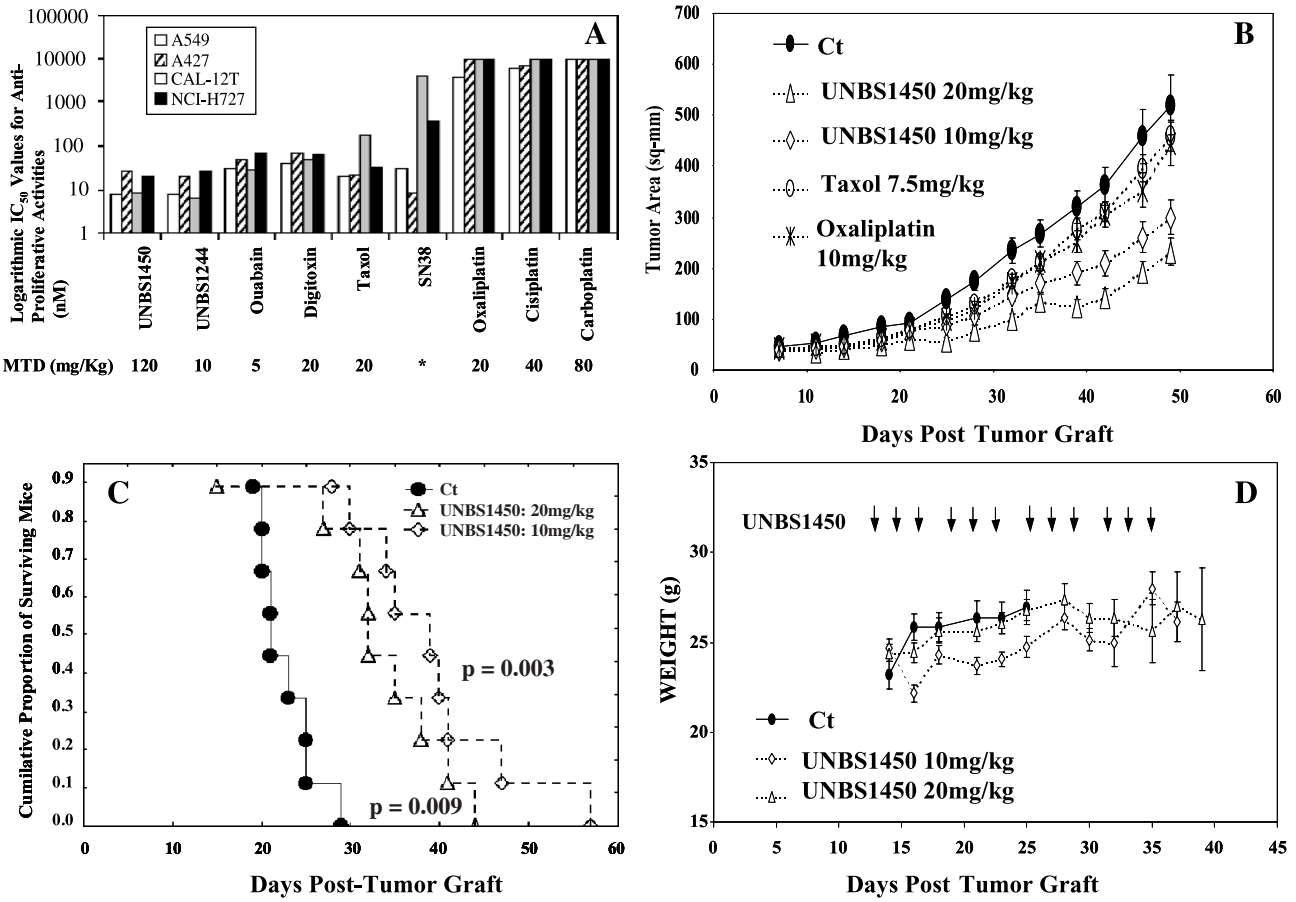

Figure 2. *In vitro and in vivo UNBS1450-mediated antitumor effects. (A) In vitro antitumor effects contributed by four cardenolides (UNBS1450, UNBS1244, ouabain, and digitoxin) relative to the four human NSCLC cell lines A549 (open bars), A427 (hatched bars), CAL-12T (gray bars), and NCI-H727 (black bars), in comparison with the five anticancer drugs already assayed against NSCLCs [i.e., paclitaxel, SN-38 (the active metabolite of irinotecan), cisplatin, oxaliplatin, and carboplatin]. The drugs (X axis) were assayed at nine concentrations ranging from 10^{-9} to 10^{-5} M, with semi-log concentration increases; each concentration was analyzed six times. The results are presented as IC_{50} values (the Y axis in logarithmic values) representing the concentrations at which each compound reduced the overall growth rate of the cell lines by 50% after 3 days of treatment. The MTD for each compound is given at the bottom of (A). MTDs are expressed in milligrams per kilogram following a single intraperitoneal administration (except for paclitaxel, which was given as a single intravenous administration) to healthy mice. Note that SN-38 (*) was tested in vitro only. (B and C) Illustration of in vivo–mediated UNBS1450 effects on the tumor growth rates of NCI-H727 NSCLC subcutaneous xenografts (B) and on the survival periods of A549 NSCLC orthotopic xenograft–bearing mice (C). Also illustrated are paclitaxel-mediated (7.5 mg/kg; open dots; B) and oxaliplatin-mediated (10 mg/kg; crosses; B) effects on NCI-H727 xenograft growth rates (B). Paclitaxel was assayed intravenously (B), whereas oxaliplatin (B) and UNBS1450 (B and C) were assayed intraperitoneally. All compounds were injected thrice a week (on Mondays, Wednesdays, and Fridays) for four consecutive weeks, with the first treatment starting on the 14th day after tumor graft. The control mice that received the vehicle are symbolized by black dots. Each experimental group consisted of nine mice. (D) The effects of UNBS1450 on mouse body weight as a check on UNBS1450-associated toxic side effects. UNBS1450 was injected intraperitoneally into A549 NSCLC orthotopic xenograft–bearing mice thrice a week (on Mondays, Wednesdays, and Fridays) for four consecutive weeks. The treatment started on the 14th day after tumor graft. The control mice that received the vehicle are symbolized by black dots. Each experimental group consisted of nine mice. The administration schedules are the same for tumor growth rates (B), animal survival (C), and weight monitoring (D).*

well-known cardenolides, such as ouabain and digitoxin, at the molecular level in terms of several characteristics: 1) its sugar moiety is linked twice to the steroid backbone, whereas ouabain and digitoxin are linked only once; 2) the molecular structure of the sugar moiety of UNBS1244 differs from those of ouabain and digitoxin because of the presence of a thiazolidinone at the 3′ end of the sugar moiety; and 3) the A/B cyclic junction is *cis* for ouabain and digitoxin, whereas it is *trans* for UNBS1244 (Figure 1). UNBS1450 differs from UNBS1244 by one chemical substituent only, namely, the hydroxyl in position 19 of the steroid skeleton in UNBS1450 compared to the formyl in the same position in UNBS1244 (Figure 1). Although this chemical modification led to a significant decrease in the *in vivo* toxicity of UNBS1450 compared to that of UNBS1244 (Figure 2*A*, *bottom*, MTD values), it nevertheless maintained the *in vitro* level of the antitumor activity of UNBS1450 compared to that of UNBS1244 (Figure 2*A*). However, it should be emphasized that poor solubility might lead to the precipitation of compounds *in vivo* and to an overestimated MTD. Solubility analyses revealed that UNBS1450 is four times more soluble than UNBS1244 in a DMSO (10%)/H_2O (90%) solution and is even more soluble than UNBS1244 in an ethanol (40%)/polyethylene glycol (40%)/H_2O (20%) solution. We are currently performing preformulation studies to arrive at the best way possible to solubilize UNBS1450 for *in vivo* experiments.

The data in Figure 2*A* indicate that, in four different NSCLC cell lines *in vitro*, UNBS1244 and UNBS1450 exhibited IC_{50} values similar to those for ouabain, digitoxin, and paclitaxel, whereas SN-38 (the active metabolite of

irinotecan) appeared to be less active. The three platin derivatives were actually less active *in vitro* than the remaining compounds under study (Figure 2*A*).

UNBS1450 Induces Significant In Vivo Antitumor Activity in Relation to Human NSCLC Xenografts

Whereas UNBS1450 significantly ($P < .01$, on the 49th day after tumor graft) decreased the tumor growth rate in the subcutaneous NCI-H727 xenograft model, paclitaxel and oxaliplatin did not (Figure 2*B*). Twelve intraperitoneal administrations of 10 mg/kg UNBS1450 led to a similar level of antitumor activity as 12 intraperitoneal administrations of 20 mg/kg (for a precise experimental schedule, refer to Figure 2*B*). UNBS1450 also significantly increased the survival periods of human A549 orthotopic NSCLC xenograft–bearing mice (Figure 2*C*) treated with 10- or 20-mg/kg dose schedules; no statistically significant ($P > .05$) differences were observed between the curves obtained with a 10-mg/kg dose schedule and the curves obtained with a 20-mg/kg dose schedule (Figure 2*C*). In contrast, we reported previously that 12 administrations of 5 mg/kg UNBS1450 (compared to 10 and 20 mg/kg) induced weaker (but nevertheless statistically significant; $P < .05$) therapeutic effects [12]. When administered per os, UNBS1450 was also able to bring about a beneficial therapeutic effect in the case of the orthotopic A549 model [12]. With respect to the reference compounds used to treat NSCLC patients, only irinotecan tended ($P = .06$) in the direction of an increase in the survival periods of human A549 orthotopic NSCLC xenograft–bearing mice, as previously reported in Mathieu et al. [7]. We previously showed that intraperitoneal/intravenous administration of paclitaxel and intraperitoneal administration of oxaliplatin do not offer any significant therapeutic effect in the case of A549 NSCLC model [7], a phenomenon also observed in the present study.

We monitored the weights of the A549 NSCLC orthotopic xenograft–bearing mice to assess the toxic side effects associated with chronic UNBS1450 treatment of tumor-bearing mice. Figure 2*D* shows that chronic treatment (12 intraperitoneal administrations) with 10 or 20 mg/kg UNBS1450 did not significantly modify the weight profile evolution of the mice bearing the A549 xenografts, thus suggesting that UNBS1450 did not produce any major toxic effects at the dose range of 10–20 mg/kg—the same ones that offer actual antitumor effects (Figure 2, *B* and *C*).

UNBS1450-Induced Antitumor Effects Relate to Its Inhibitory Effects on Na^+/K^+ ATPase Activity

For Na^+/K^+ ATPase activity assay, we used a purified cerebral cortex porcine Na^+/K^+ ATPase because of the great similarity between the porcine α_1 subunit and the human α_1 subunit (amino acid sequence alignments indicate a 99% similarity between these two proteins). Figure 3 clearly shows that UNBS1450 has a greater inhibitory effect on sodium pump activity than ouabain or digitoxin. The IC_{50} values of UNBS1450, ouabain, and digitoxin in terms of the inhibition of sodium pump activity (Figure 3) are in the same ranges as the IC_{50} values obtained in terms of antiproliferative effects (Figure 2*A*). These data therefore suggest that the UNBS1450-related antitumor effects detailed in the present study are at least partly related to UNBS1450-induced inhibition of sodium pump activity.

UNBS1450 Causes a Time-Dependent and Dose-Dependent Increase in Non–Apoptotic-Related A549 Cell Death

Although the number of cardenolides has been reported as inducing apoptosis (in micromolar dose ranges) in human prostate cancer cells [32–36], we did not observe any such features with UNBS1450 (in nanomolar dose ranges, corresponding to IC_{50}) in the case of human A549 NSCLC cells (Figures 4, *A*–*E*) nor, indeed, in that of NCI-H727 cells (data not shown). We used flow cytometry analysis to monitor the effect of 1, 10, and 100 nM UNBS1450 on A549 cell death over 24 and 72 hours (Figure 4, *A* and *B*). PARP cleavage analysis (10 and 100 nM UNBS1450 in Figure 4, *C* and *D*, respectively) only revealed the presence of intact (uncleaved) PARP (molecular mass, 116 kDa), whereas fragments representative of apoptosis (83–89 kDa) and necrosis (50–60 kDa) were absent. In fact, 10- and 100-nM doses of UNBS1450 caused a time- and dose-dependent increase in non–apoptotic-related A549 cell death (Figure 4, *A* and *B*)—a feature observed in the case of NCI-H727 NSCLC cells (data not shown). We decided to work with nanomolar, instead of micromolar, doses of UNBS1450 because the IC_{50} window for UNBS1450 in the antiproliferative assay is in the nanomolar range (Figure 2*A*). To offer the ultimate experimental proof of the fact that UNBS1450 does not induce apoptosis in A549 NSCLC cells, we also performed TUNEL analysis because positive staining for both PI and Annexin V may occur late in the process, leading to apoptotic cell death in some instances. The data illustrated in Figure 4*E* once more indicate that UNBS1450 does not induce any apoptotic feature in A549 NSCLC cells.

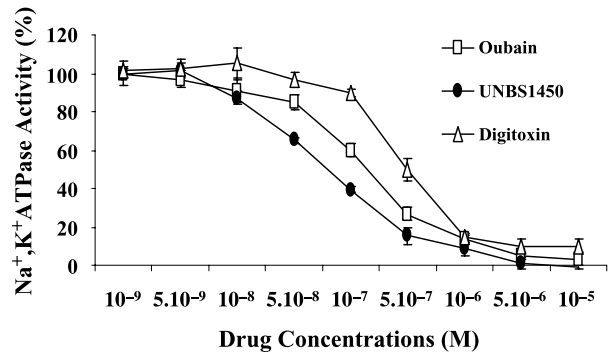

Figure 3. *UNBS1450 inhibits Na^+/K^+ ATPase activity. The effects of UNBS1450, ouabain, and digitoxin on sodium pump activity were characterized by the use of the purified porcine cerebral cortex Na^+/K^+ ATPase. The activity of the porcine sodium pump in the absence of cardiotonic steroids was arbitrarily normalized to 100% (Y axis). Concentrations ranging from 1 to 10,000 nM were analyzed (X axis). Each concentration was analyzed in sextuplicate.*

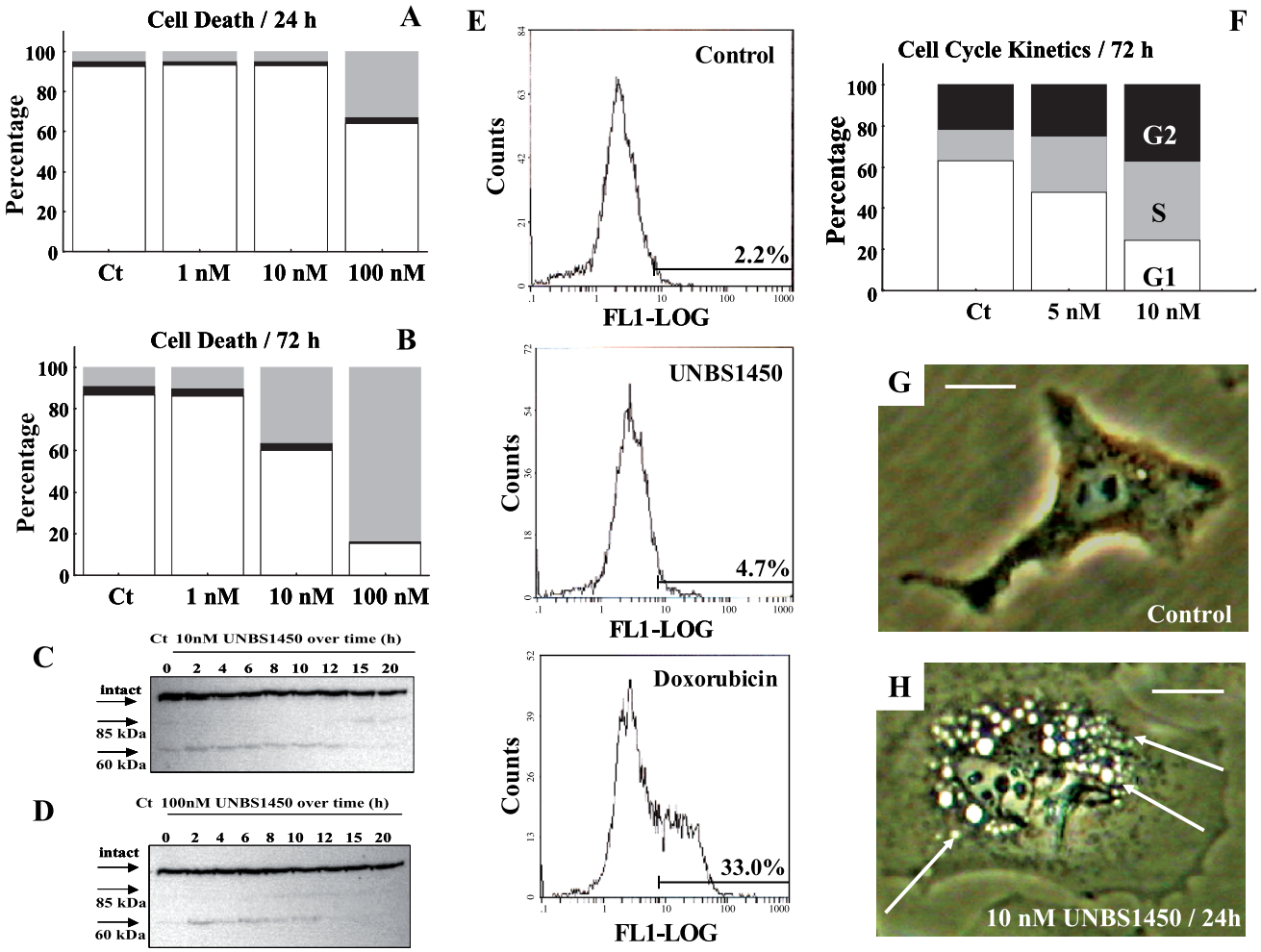

Figure 4. *UNBS1450 causes a time- and dose-dependent increase in non–apoptotic-related A549 cell death. Characterization of UNBS1450-induced effects with respect to the level of cell death (monitored by flow cytometry) over 24 hours (A) and 72 hours (B); the open bars represent normal cells, whereas the black and gray bars represent apoptotic and nonapoptotic cells, respectively. (C and D) Effects of 10 and 100 nM UNBS1450 over a period of 20 hours on the cleavage pattern of PARP; intact (uncleaved) PARP has a molecular mass of 116 kDa. (E) TUNEL analyses were performed to confirm the absence of UNBS1450-induced apoptosis in A549 NSCLC cells. A549 cells were incubated for 72 hours in the presence of 2.5 μM doxorubicin (positive control) or 10 nM UNBS1450. Control cells were incubated with the solvent alone. The percentage of TUNEL-positive cells in each condition is reported. (F) The cell cycle kinetics was monitored by flow cytometry over 72 hours; the open bars represent the proportion of A549 cells in the G_1 phase of their cell cycles, whereas the gray and black bars represent the proportion of A549 cells in the S and G_2 phases, respectively. Each experiment was carried out in triplicate, and panels A, B, and F illustrate the net results obtained after the combination of triplicates. (G and H) Illustration of marked cytoplasmic vacuole formation (indicated by white arrows) in A549 NSCLC cells over a 24-hour period of UNBS1450 treatment. White bars represent 15 μm. The magnification is the same in (G) and (H).*

UNBS1450 Induces Cell Cycle Arrest in S Phase

In addition to the data already contributed by the MTT colorimetric assay (Figure 2*A*), we used a flow cytometry approach to characterize the antiproliferative effects observed with UNBS1450 (Figure 4*F*). The data in Figure 4*F* show that 10 nM UNBS1450 markedly increased the percentage of A549 cells in the S phase of the cell cycle and, to a lesser extent, in the G_2 phase.

UNBS1450 Induces Vacuolization-Related Cell Death in A549 Tumor Cells

The flow cytometry–related analyses detailed in Figure 4, *A* and *B*; the PARP analyses in Figure 4, *C* and *D*; and the TUNNEL analysis in Figure 4*E* show that UNBS1450-mediated cell death occurs through a non–apoptotic-related cell death process. Computer-assisted videomicroscopy analysis further revealed that UNBS1450 did not kill the A549 NSCLC cells by osmotic shock (data not shown). In addition, this analysis strongly suggests that UNBS1450 did not induce necrotic-related A549 cell death (data not shown)—an assertion corroborated by the fact that PI heavily stained the A549 cell nuclei, a feature observed during flow cytometry analyses for apoptotic measurements (Figure 4, *A* and *B*). When dying cells still stain heavily with PI, necrotic processes are unlikely to occur [3,5]. Two additional arguments in favor of the finding that UNBS1450 does not induce necrotic-related cell death are as follows: firstly, *in vivo*, UNBS1450 did not increase the proportion of necrotic areas in the NCI-H727 and A549 xenografts (data not shown); secondly, UNBS1450 treatment did not

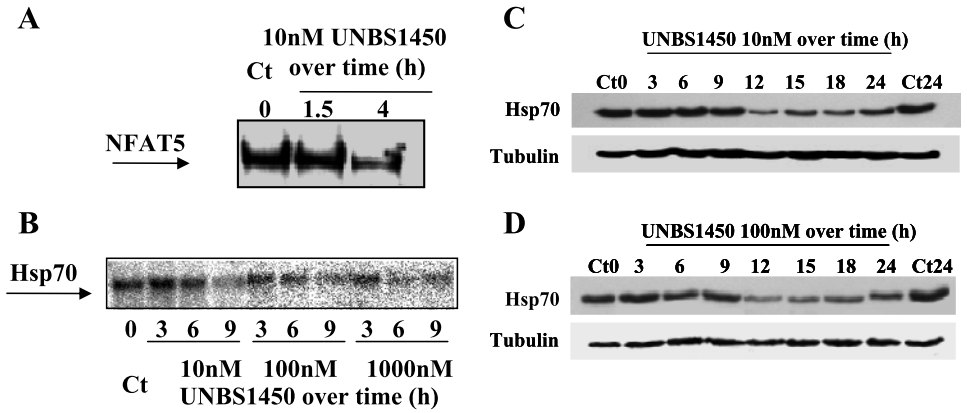

Figure 5. *UNBS1450 induces Hsp70 downregulation. (A) Characterization (Western blot analyses) of NFAT5/TonEBP protein accumulation in untreated and UNBS1450-treated (10 nM) A549 cells. (B) Determination (Northern blot analyses) of 10, 100, and 1000 nM UNBS1450-mediated effects on Hsp70 mRNA accumulation over a period of 9 hours (lower panel). (C and D) Effects of 10 and 100 nM UNBS1450 treatment on the accumulation of Hsp70 in A549 tumor cells.*

bring about a PARP cleavage that yielded fragments of 50 to 62 kDa (specific for necrosis features), as shown in Figure 4, *C* and *D*. Thus, UNBS1450 does not seem to induce either apoptotic-related or necrotic-related cell death in A549 NSCLC cells, but rather a cell death process associated with a dramatic cytoplasmic vacuolization revealed by computer-assisted videomicroscopy (Figure 4, *G* and *H*).

UNBS1450 Induces Hsp70 Downregulation

One of the anti–cell death mechanisms active in lung cancer cells involves the overexpression of Hsp70 [21], which fulfills its prosurvival function by inhibiting LMP [22]. Nylandsted et al. [37] have reported that the abrogation of Hsp70 synthesis by the adenoviral transfer of a fragment of Hsp70 cDNA resulted in extensive cell death in several breast cancer cell lines, and that this cell death–associated effect is clearly different from the standard apoptosis pathway. Frese et al. [21] have shown that selective downregulation of Hsp70 induces massive caspase-independent tumor cell death in lung cancer, but not in normal lung cells. Hsp70 is under the transcriptional control of the activator, NFAT5/TonEBP [38]. Its activity is affected by Na^+/K^+ balance, and its downregulation by ouabain has already been evidenced [39]. As revealed by Western blot analyses, 10 nM UNBS1450 decreases NFAT5 protein levels (Figure 5*A*). This effect leads to a decrease of the Hsp70 both at the mRNA level (as revealed by Northern blot analyses; Figure 5*B*) and at the protein level (as revealed by Western blot analyses; 10 and 100 nM, in Figure 5, *C* and *D*, respectively).

UNBS1450 Induces LMP-Mediated Cell Death

As indicated above, Hsp70 fulfils its prosurvival function by inhibiting LMP [22]. Recent data indicate that lysosomes also function as death signal integrators that mediate caspase-independent and/or apoptosis-inducing factor–independent PCD [23,24]. The permeabilization of lysosomes was analyzed by measuring the emission of green fluorescence, which is indicative of the leakage of acridine orange from the acidic compartment to the cytosol, as described by Nylandsted et al. [22]. In this experiment, cells were stained with acridine orange and either left untreated or treated with 10 nM UNBS1450 for 15 hours. As shown in Figure 6, UNBS1450 treatment induced a marked increase in green fluorescence, and we demonstrated the influence of UNBS1450 on lysosomal permeabilization. Furthermore, immunofluorescent staining for cathepsin B (Figure 7) showed a distinct pattern for untreated cells (concentrated, punctuated staining; Figure 7*B*), in comparison with UNBS1450-treated cells with diffuse cathepsin B staining (Figure 7*D*), and thus revealed leakage of lysosomes.

Discussion

Apart from their well-known effects in congestive heart failure [13], cardenolides have also been reported as having potent anti-inflammatory [40,41] and antitumor [42–44] effects, especially on human prostate [32–35] and breast [14,45] cancers. Xenavex, an ethanolic botanical extract compound

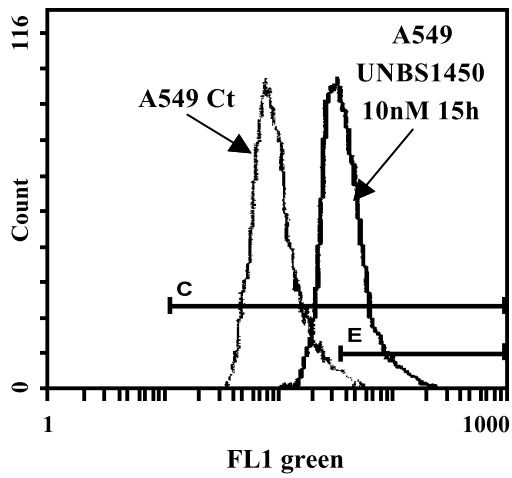

Figure 6. *UNBS1450 induces LMP in human A549 NSCLC cells. UNBS1450-induced permeabilization of lysosomes, as analyzed by measuring the emission of green fluorescence (flow cytometry), which is indicative of the leakage of acridine orange from the acidic compartment to the cytosol. The Y axis represents the number of counted events (cells), whereas the X axis represents green fluorescence intensity (in logarithmic scale).*

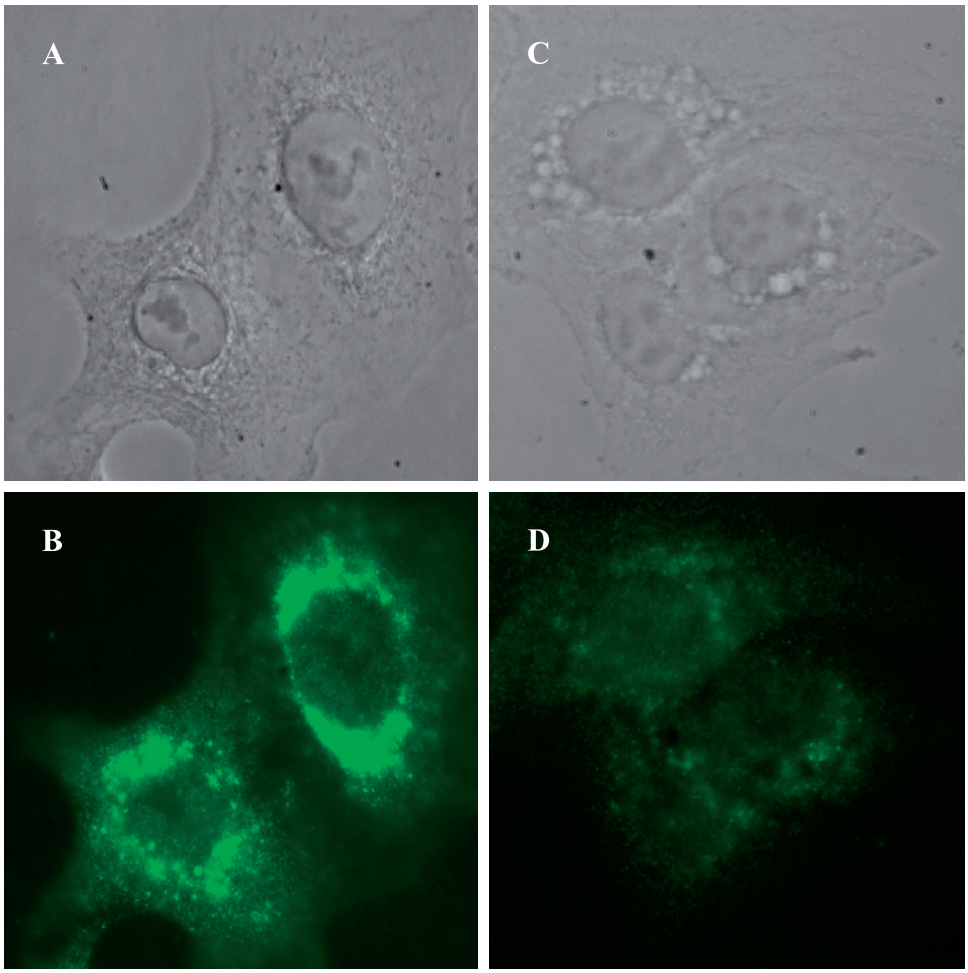

Figure 7. *UNBS1450 induces LMP-mediated cell death in human A549 NSCLC cells. Immunofluorescent staining for cathepsin B in untreated A549 cells (B; with A representing the corresponding phase contrast image) in comparison with A549 cells treated for 15 hours with 10 nM UNBS1450 (D; with C representing the corresponding phase contrast image).*

of various cardioglycosides (with an enriched fraction of oleandrin) derived from *Nerium oleander*, is entering a multicenter phase I/II clinical trial program as a potential monotherapy for NSCLC (for details, see http://clinicaltrial.gov). Both the data from the present study and those that we reported previously [12,25] introduce UNBS1450, a novel cardenolide (Figure 1), as a novel anticancer drug with real potential for the treatment of NSCLCs. Indeed, both the data from the present study and the data from previous studies [12,25] clearly indicate that UNBS1450 has a number of marked antitumor effects, both *in vitro* and *in vivo*, on various aggressive models of human NSCLCs.

In a previous study [12], we observed that some of the NSCLC antitumor effects induced by UNBS1450 are linked to the inactivation of the NF-κB pathway. As indicated in the Introduction, the NF-kB and Hsp70 pathways are intimately related [17–20]; in the present study, we therefore focused our attention on a specific target for UNBS1450 in the shape of Hsp70. One of the anti–cell death mechanisms active in lung cancer cells involves the overexpression of Hsp70. Its high level of expression in various human tumors correlates with resistance to therapy and poor prognosis [21,46,47]. Nylandsted et al. [48] have demonstrated that the locoregional application of an adenovirus expressing antisense Hsp70 cDNA (AdasHsp70) eradicates orthotopic xenografts of glioblastomas and breast carcinomas, and subcutaneous xenografts of colon carcinomas in immunodeficient mice. Moreover, Frese et al. [21] have shown that selective downregulation of Hsp70 induces cell death in lung cancer, but not in normal lung cells. The depletion of Hsp70 is therefore an effective means of combating cancer. However, its downregulation by adenoviral transfer is quite unsuitable for clinical application in humans. We show here that the novel anticancer drug UNBS1450 decreases the levels of both Hsp70 mRNA and protein, and thus could be used more efficiently for anti-Hsp70–based therapy. The transcriptional control of Hsp70 involves the transcriptional activator, NFAT5/TonEBP [38]. We also show that UNBS1450 decreases the level of expression of NFAT5/TonEBP in A549 tumor cells. Similar *in vitro* effects have previously been reported for another cardenolide (ouabain) in Madin-Darby canine kidney cells [39]. However, in the study reported by Neuhofer et al. [39], data indicate that the regulation of the Hsp70 promoter by ouabain is more complex than that of

other TonEBP target genes. At present, we cannot give any precise explanation on the relationship between TonEBP and Hsp70, on one hand, and UNBS1450 action in human A549 NSCLCs, on the other hand. We will adopt a genomic and proteomic approach to offer an explanation, however incomplete, of this specific point. In addition, we have not yet proven that UNBS1450 downregulates Hsp70 directly. An assay based on Hsp70 overexpression may provide promising evidence—a strategy we are currently involved in. Indeed, Nylandsted et al. [37] reported that the abrogation of Hsp70 synthesis by the adenoviral transfer of a fragment of Hsp70 cDNA resulted in extensive cell death in several breast cancer cell lines, and that this cell death–associated effect was clearly different from the standard apoptosis pathway. In the present study, we also show that UNBS1450-induced cell death is nonapoptotic. In using flow cytometry to characterize the antiproliferative effects of UNBS1450 on A549 NSCLC cells, we observed that this compound markedly increased the percentage of A549 cells in the S phase of the cell cycle and, to a lesser extent, in the G_2 phase. We then employed a dedicated microarray approach for the preliminary characterization of UNBS1450-induced increment in S-phase A549 cells. These preliminary data suggest that the UNBS1450-induced increase in S-phase A549 cells could relate to a marked decrease in the mRNA levels of cdc25B and cdc25C (data not shown). Kometiani et al. [49] have shown that ouabain concentrations (100 nM or lower) causing a < 25% inhibition in the pumping function of the sodium pump have no effect on cell viability but do inhibit proliferation. At the same concentrations, ouabain: 1) activates Src kinase and stimulates the interaction of Src and Na^+/K^+ ATPase with the EGFR; 2) causes transient activation and then a sustained activation of extracellular signal–regulated kinases 1 and 2 (ERK1/2); 3) increases the expression of p21Cip1, but decreases that of p53; and 4) activates c-Jun NH_2-terminal kinase, but not p38 kinase [49]. Taken together, all these data suggest that ouabain-induced activation/transactivation of Src/EGFR by the sodium pump leads to the activation of ERK1/2, a resulting increase in the level of cell cycle inhibitor p21Cip1, and growth arrest. We are currently performing experiments to investigate whether UNBS1450 has any similar effects on A549 NSCLC cells.

Hsp70 fulfils its prosurvival function by inhibiting LMP [22–24,47], a perturbation of a lysosomal membrane function that leads to the release of lysosomal hydrolases (including cathepsins) in the cell cytoplasm [22]. The marked changes that occur in the lysosomal compartment during cell transformation and the involvement of lysosomal enzymes in death pathways that remain functional in advanced tumor cells suggest that the lysosomal death pathway could contribute significantly to programmed sensitivity to cell death in cancer cells [23,24]. Furthermore, because LMP-induced cell death is caspase- and apoptosis-independent, it is a very interesting target in cancer therapy because it allows cell death to occur even in cancer cells with multiple defects in the normal apoptosis pathway. In this study, we show that UNBS1450 induces LMP followed by a release of cathepsin B in the A549 cell cytoplasm (Figures 6 and 7). The exact mechanism by which Hsp70 inhibits LMP remains to be deciphered. Because Hsp70 depletion from tumor cells—but not from normal cells—triggers LMP, one might speculate that Hsp70 is required for the stability of tumor-specific subpopulations of lysosomes. In line with this, it is important to note that Hsp70 is confined to endolysosomal membranes in cancer cells and prevents both spontaneous and TNF- and etoposide-induced LMP [22,47]. Furthermore, one cell-related function already evidenced in Hsp70 is the facilitation of the removal of injured proteins [50,51]. Thus, the protective Hsp70 effect could be due to the removal of toxic proteins and protein aggregates.

Rosen et al. [52] recently reported that cardiac steroids induce changes in endocytosis-dependent membrane traffic, leading to the appearance of cytoplasmic vacuoles. These authors report that a cardiac steroid–induced accumulation of cytoplasmic membrane components is a result of inhibited recycling within the late endocytic pathway [52].

In conclusion, through its interaction with the sodium pump, UNBS1450 decreases the expression of Hsp70; this likely leads to LMP and, thus, to overcoming of the multiple anti–cell death mechanisms evidenced in NSCLCs, which are at least partly responsible for the failure of currently used chemotherapeutic drugs. UNBS1450 could thus be considered as a novel drug with a potential for NSCLC treatment.

References

[1] Rigas JR (2004). Taxane–platinum combinations in advanced non–small cell lung cancer: a review. *Oncologist* **9,** 16–23.

[2] Gridelli C, Maione P, Airoma G, and Rossi A (2002). Selective cyclooxygenase-2 inhibitors and non–small-cell lung cancer. *Curr Med Chem* **9,** 1851–1858.

[3] Sperandio S, de Belle I, and Bredesen DE (2000). An alternative, non-apoptotic form of programmed cell death. *Proc Natl Acad Sci USA* **97,** 14376–14381.

[4] Guo B, Hembruff SL, Villeneuve DJ, Kirwan AF, and Parissenti AM (2003). Potent killing of paclitaxel- and doxorubicin-resistant breast cancer cells by calphostin C accompanied by cytoplasmic vacuolisation. *Breast Cancer Res Treat* **82,** 125–141.

[5] Okada H and Mak TW (2004). Pathways of apoptotic and non-apoptotic death in tumour cells. *Nat Rev Cancer* **4,** 592–603.

[6] Debatin KM and Krammer PH (2004). Death receptors in chemotherapy and cancer. *Oncogene* **23,** 2950–2966.

[7] Mathieu A, Remmelink M, D'Haene N, Penant S, Gaussin JF, Van Ginckel R, Darro F, Kiss R, and Salmon I (2004). Development of a chemoresistant orthotopic human non–small cell lung carcinoma model in nude mice. *Cancer* **101,** 1908–1918.

[8] Lee HY, Srinivas H, Xia D, Lu Y, Superty R, LaPushin R, Gomez-Manzano C, Gal AM, Walsh GL, Force T, et al. (2003). Evidence that phosphatidylinositol 3-kinase– and mitogen-activated protein kinase kinase-4/c-Jun NH_2-terminal kinase–dependent pathways cooperate to maintain lung cancer cell survival. *J Biol Chem* **278,** 23630–23638.

[9] Castillo SS, Brognard J, Petukhov PA, Zhang C, Tsurutani J, Granville CA, Li M, Jung M, West KA, Gills JG, et al. (2004). Preferential inhibition of Akt and killing of Akt-dependent cancer cells by rationally designed phosphatidylinositol ether lipid analogues. *Cancer Res* **64,** 2782–2792.

[10] Mayo MW, Denlinger CE, Broad RM, Yeung F, Reilly ET, Shi Y, and Jones DR (2003). Ineffectiveness of histone deacetylase inhibitors to induce apoptosis involves the transcriptional activation of NF-kappa B through the Akt pathway. *J Biol Chem* **278,** 18980–18989.

[11] Pommier Y, Sordet O, Antony S, Hayward RL, and Kohn KW (2004). Apoptosis defects and chemotherapy resistance: molecular interaction maps and networks. *Oncogene* **23,** 2934–2949.

[12] Mijatovic T, Op De Beeck A, Van Quaquebeke E, Dewelle J, Darro F, de Launoit Y, and Kiss R (2006). The cardenolide UNBS1450 is able to deactivate NF-κB–mediated cytoprotective effects in human non–small-cell-lung cancer (NSCLC) cells. *Mol Cancer Ther* **5,** 391–399.

[13] Dmitrieva RI and Doris PA (2002). Cardiotonic steroids: potential endogenous sodium pump ligands with diverse function. *Exp Biol Med* **227,** 561–569.
[14] Stenkvist B, Pengtsson E, Dahlquist B, Eriksson O, Jarkrans T, and Nordin B (1982). Cardiac glycosides and breast cancer, revisited. *N Engl J Med* **306,** 484.
[15] Xie Z and Askari A (2002). Na^+/K^+-ATPase as a signal tranducer. *Eur J Biochem* **269,** 2434–2439.
[16] Wang H, Haas M, Liang M, Cai T, Tian J, Li S, and Xie Z (2004). Ouabain assembles signaling cascades through the caveolar Na^+/K^+-ATPase. *J Biol Chem* **279,** 17250–17259.
[17] Guzhova IV, Darieva ZA, Melo AR, and Margulis BA (1997). Major stress protein Hsp70 interacts with NF-kB regulatory complex in human T-lymphoma cells. *Cell Stress Chaperones* **2,** 132–139.
[18] Asea A, Rehli M, Kabingu E, Boch JA, Bare O, Auron PE, Stevenson MA, and Calderwood SK (2002). Novel signal transduction pathway utilized by extracellular Hsp70: role of toll-like receptor (TLR) 2 and TLR4. *J Biol Chem* **277,** 15028–15034.
[19] Li X, Hua L, Deng F, Bai X, Zeng W, Lu D, Su Y, and Luo S (2005). NF-kappaB and Hsp70 are involved in the phospholipase C gamma1 signaling pathway in colorectal cancer cells. *Life Sci* **77,** 2794–2803.
[20] King TA, Ghazalech RA, Juhn SK, Adams GL, and Ondrey FG (2005). Induction of heat shock protein 70 inhibits NF-kappa-B in squamous cell carcinoma. *Otolaryngol Head Neck Surg* **133,** 70–79.
[21] Frese S, Schaper M, Kuster JR, Miescher D, Jaattela M, Buehler T, and Schmid RA (2003). Cell death induced by down-regulation of heat shock protein 70 in lung cancer cell lines is p53-independent and does not require DNA cleavage. *J Thorac Cardiovasc Surg* **126,** 748–754.
[22] Nylandsted J, Gyrd-Hansen M, Danielewicz A, Fehrenbacher N, Lademann U, Hoyer-Hansen M, Weber E, Multhoff G, Rohde M, and Jaattela M (2004). Heat shock protein 70 promotes cell survival by inhibiting lysosomal membrane permeabilization. *J Exp Med* **200,** 425–435.
[23] Jaattela M (2004). Multiple cell death pathways as regulators of tumour initiation and progression. *Oncogene* **23,** 2746–2756.
[24] Fehrenbacher N and Jaattela M (2005). Lysosomes as targets for cancer therapy. *Cancer Res* **65,** 2993–2995.
[25] Van Quaquebeke E, Simon G, Andre A, Dewelle J, Yazidi ME, Bruyneel F, Tuti J, Nacoulma O, Guissou P, Decaestecker C, et al. (2005). Identification of a novel cardenolide (2″-oxovorusharin) from *Calotropis procera* and the hemisynthesis of novel derivatives displaying potent *in vitro* antitumor activities and high *in vivo* tolerance: structure–activity relationship analyses. *J Med Chem* **48,** 849–856.
[26] Camby I, Salmon I, Danguy A, Pasteels JL, Brotchi J, Martinez J, and Kiss R (1996). Influence of gastrin on human astrocytic tumor cell proliferation. *J Natl Cancer Inst* **88,** 594–600.
[27] Darzynkiewicz Z, Juan G, Li X, Gorczyca W, Murakami T, and Traganos F (1997). Cytometry in cell neurobiology: analysis of apoptosis and accidental cell death (necrosis). *Cytometry* **27,** 1–20.
[28] Maecker HL, Koumenis C, and Giaccia AJ (2000). p53 promotes selection for Fas-mediated apoptotic resistance. *Cancer Res* **60,** 4638–4644.
[29] de Launoit Y, Veilleux R, Dufour M, Simard J, and Labrie F (1991). Characteristics of the biphasic action of androgens and of the potent antiproliferative effects of the new pure antiestrogen EM-139 on cell cycle kinetic parameters in LNCaP human prostatic cancer cells. *Cancer Res* **51,** 5165–5170.
[30] Mathieu V, Mijatovic T, van Damme M, and Kiss R (2005). Gastrin exerts pleiotropic effects on human melanoma cell biology. *Neoplasia* **7,** 930–943.
[31] Kiss R, de Launoit Y, Danguy A, Paridaens R, and Pasteels JL (1989). Influence of pituitary grafts or prolactin administrations on the hormone sensitivity of ovarian hormone-independent mouse mammary MXT tumors. *Cancer Res* **49,** 2945–2951.
[32] McConkey DJ, Lin Y, Nutt LK, Ozel HZ, and Newman RA (2000). Cardiac glycosides stimulate Ca^{2+} increases and apoptosis in androgen-independent, metastatic human prostate adenocarcinoma cells. *Cancer Res* **60,** 3807–3812.
[33] Yeh JY, Huang WJ, Kan SF, and Wang PS (2001). Inhibitory effects of digitalis on the proliferation of androgen dependent and independent prostate cancer cells. *J Urol* **166,** 1937–1942.
[34] Yeh JY, Huang WJ, Kan SF, and Wang PS (2003). Effects of bufalin and cinobufagin on the proliferation of androgen dependent and independent prostate cancer cells. *Prostate* **54,** 112–124.
[35] Huang YT, Chueh SC, Teng CM, and Guh JH (2004). Investigation of ouabain-induced anticancer effect in human androgen-independent prostate cancer PC-3 cells. *Biochem Pharmacol* **67,** 727–733.
[36] Lin H, Juang JL, and Wang PS (2004). Involvement of Cdk5/p25 in digoxin-triggered prostate cancer cell apoptosis. *J Biol Chem* **279,** 29302–29307.
[37] Nylandsted J, Rohde M, Brand K, Bastholm L, Elling F, and Jaattela M (2000). Selective depletion of heat shock protein 70 (Hsp70) activates a tumor-specific death program that is independent of caspases and bypasses Bcl-2. *Proc Natl Acad Sci USA* **97,** 7871–7876.
[38] Na KY, Woo SK, Lee SD, and Kwon HM (2003). Silencing of TonEBP/NFAT5 transcriptional activator by RNA interference. *J Am Soc Nephrol* **14,** 283–288.
[39] Neuhofer W, Woo SK, Na KY, Grunbein R, Park WK, Nahm O, Beck FX, and Kwon HM (2002). Regulation of TonEBP transcriptional activator in MDCK cells following changes in ambient tonicity. *Am J Physiol Cell Physiol* **283,** C1604–C1611.
[40] Manna SK, Sah NK, Newman RA, Cisneros A, and Aggarwal BB (2000). Oleandrin suppresses activation of nuclear transcription factor-kappaB, activator protein-1, and c-Jun NH_2-terminal kinase. *Cancer Res* **60,** 3838–3847.
[41] Srivastava M, Eidelman O, Zhang J, Paweletz C, Caohuy H, Yang Q, Jacobson KA, Heldman E, Huang W, Jozwik C, et al. (2004). Digitoxin mimics gene therapy with CFTR and suppresses hypersecretion of IL-8 from cystic fibrosis lung epithelial cells. *Proc Natl Acad Sci USA* **101,** 7693–7698.
[42] Inada A, Nakanishi T, Konoshima T, Kozuka M, Tokuda H, Nishino H, and Iwashima A (1993). Anti-tumor promoting activities of natural products: II. Inhibitory effects of digitoxin on two-stage carcinogenesis of mouse skin tumors and mouse pulmonary tumors. *Biol Pharm Bull* **16,** 930–931.
[43] Afaq F, Saleem M, Aziz MH, and Mukhtar H (2004). Inhibition of 12-*O*-tetradecanoylphorbol-13-acetate–induced tumor promotion markers in CD-1 mouse skin by oleandrin. *Toxicol Appl Pharmacol* **195,** 361–369.
[44] Stenkvist B (2001). Cardenolides and cancer. *Anticancer Drugs* **12,** 635–638.
[45] Chen JQ, Contreras RG, Wang R, Fernandez SV, Shoshani L, Ruso IH, Cerijido M, and Russo J (2006). Sodium/potassium ATPase (Na(+),K(+)-ATPase) and ouabain/related cardiac glycosides: a new paradigm for development of anti–breast cancer drugs? *Breast Cancer Res Treat* **96,** 1–15.
[46] Jäättela M (1999). Heat shock proteins as cellular lifeguards. *Ann Med* **31,** 261–271.
[47] Gyrd-Hansen M, Nylandsted J, and Jaattela M (2004). Heat shock protein 70 promotes cancer cell viability by safeguarding lysosomal integrity. *Cell Cycle* **3,** 1484–1485.
[48] Nylandsted J, Wick W, Hirt UA, Brand K, Rohde M, Leist M, Weller M, and Jaattela M (2002). Eradication of glioblastoma, and breast and colon carcinoma xenografts by Hsp70 depletion. *Cancer Res* **62,** 7139–7142.
[49] Kometiani P, Liu L, and Askari A (2005). Digitalis-induced signalling by Na^+/K^+-ATPase in human breast cancer cells. *Mol Pharmacol* **67,** 929–936.
[50] Doong H, Rizzo K, Fang S, Kulpa V, Weissman AM, and Kohn EC (2003). CAIR-1/BAG-3 abrogates heat shock protein-70 chaperone complex–mediated protein degradation. *J Biol Chem* **278,** 28490–28500.
[51] Chiang HL, Terlecky S, Plant CP, and Dice JF (1989). A role for a 70-kilodalton heat shock protein in lysosomal degradation of intracellular proteins. *Science* **246,** 382–385.
[52] Rosen H, Glukhman V, Feldmann T, Fridman E, and Lichtstein D (2004). Cardiac steroids induce changes in recycling of the plasma membrane in human NT2 cells. *Mol Biol Cell* **15,** 1044–1054.